Rapid Communications

Ferromagnetic Peierls insulator state in AMg$_4$Mn$_6$O$_{15}$ (A = K,Rb,Cs)

T. Yamaguchi,[1] K. Sugimoto,[2] Y. Ohta,[1] Y. Tanaka,[3] and H. Sato[3]
[1]*Department of Physics, Chiba University, Chiba 263-8522, Japan*
[2]*Center for Frontier Science, Chiba University, Chiba 263-8522, Japan*
[3]*Department of Physics, Chuo University, Tokyo 112-8551, Japan*

(Received 16 February 2018; published 5 April 2018)

Using the density-functional-theory-based electronic structure calculations, we study the electronic state of recently discovered mixed-valent manganese oxides AMg$_4$Mn$_6$O$_{15}$ (A = K,Rb,Cs), which are fully spin-polarized ferromagnetic insulators with a cubic crystal structure. We show that the system may be described as a three-dimensional arrangement of the one-dimensional chains of a $2p$ orbital of O and a $3d$ orbital of Mn running along the three axes of the cubic lattice. We thereby argue that in the ground state the chains are fully spin polarized due to the double-exchange mechanism and are distorted by the Peierls mechanism to make the system insulating.

DOI: 10.1103/PhysRevB.97.161103

Magnetism and electronic transport properties of materials are closely related to each other; e.g., insulating transition-metal oxides are typically antiferromagnetic, and ferromagnetism usually goes hand in hand with metallicity [1,2]. One of the rare exceptions to this rule is a hollandite chromate $K_2Cr_8O_{16}$ [3–9] where the double-exchange mechanism [10–13] induces a three-dimensional (3D) full spin polarization in the system below $T_c = 180$ K, and then the metal-insulator (MI) transition follows in its fully spin-polarized quasi-one-dimensional (1D) conduction band by the Peierls mechanism at $T_{MI} = 95$ K without affecting its 3D ferromagnetism [5,14,15]. Thus, the uncommon ferromagnetic insulating state is realized in the ground state of this material.

Recently, Tanaka and Sato [16] discovered a novel series of manganese oxides AMg$_4$Mn$_6$O$_{15}$ (A = K, Rb, and Cs), which were reported to be insulating ferromagnets with a highly symmetric body-centered-cubic structure (see Fig. 1). The Mn ions are in a mixed-valent state of Mn^{3+} and Mn^{4+} with an average oxidation state of $3.5 + (3d^{3.5})$ and are fully spin polarized in the ground state with a ferromagnetic transition temperature of $T_c \simeq 170$ K. The electric resistivity shows an insulating behavior in the entire temperature range observed (i.e., below 300 K). The materials reveal a large negative magnetoresistance: In KMg$_4$Mn$_6$O$_{15}$, the resistivity is suppressed by ~40% under 5 T of magnetic field.

In this Rapid Communication, we will show that a similar mechanism of insulating ferromagnetism to that of $K_2Cr_8O_{16}$ applies also in this manganese series. Namely, we will use the density-functional-theory- (DFT-) based electronic structure calculations to demonstrate that an unexpectedly simple electronic state resides in this series with a rather complicated crystal structure: The ground state of the system may be described as a 3D arrangement of the three 1D chains of an O $2p$ orbital and a Mn $3d$ orbital, which are $p_\alpha - d_{3\alpha^2-r^2} - p_\alpha - d_{3\alpha^2-r^2} - \cdots$ ($\alpha = x,y,z$) running along the α axis of the cubic lattice. We will argue that the calculated localized/itinerant dualistic nature of electrons in the chains leads the system to ferromagnetism due to the double-exchange mechanism. We will also predict that these chains are dimerized by the Peierls mechanism so that the system is insulating with a band gap in agreement with experiment; the system must be metallic if there were no lattice dimerizations.

We employ the WIEN2K code [17] based on the full-potential linearized augmented-plane-wave method for our DFT calculations. We present calculated results obtained in the generalized gradient approximation (GGA) for electron correlations with the exchange-correlation potential of Ref. [18]. To improve the description of electron correlations in Mn $3d$ orbitals, we use the rotationally invariant version of the GGA + U method with the double-counting correction in the fully localized limit [19,20]. In the following, we will present the results obtained at $U = 0$ and 4 eV. The spin polarization is allowed when necessary. The spin-orbit coupling is not taken into account in the following calculations, but we have checked that the spin-orbit coupling does not change our results qualitatively; e.g., the band gap does not open by the spin-orbit coupling.

We use the crystal structure measured at room temperature [16], which has the cubic symmetry [space-group $Im\bar{3}m$ (No. 229)] with the lattice constants of $a = 8.3034(4)$, 8.3049(3), and 8.3476(5) for A = K, Rb, and Cs, respectively, in units of angstroms. The primitive unit cell contains 6 Mn and 15 O ions. All the Mn ions are crystallographically equivalent, but there are two crystallographically inequivalent O ions (which we call O1 and O2). There are 12 O1 and 3 O2 ions in the primitive unit call. In the self-consistent calculations, we use $15 \times 15 \times 15$ $\boldsymbol{k}$ points in the Brillouin zone. Muffin-tin radii (R_{MT}) of 2.50 (A), 1.96 (Mg), 1.94 (Mn), and 1.67 (O) bohrs are used, and we assume the plane-wave cutoff of $K_{max} = 8.50/R_{MT}$. Because of a large R_{MT} value of the A ion, we choose the maximum value for the partial waves used in the computations of nonsphere matrix elements to be 6. We use VESTA [21] and XCRYSDEN [22] for graphical purposes.

Now, let us discuss the calculated densities of states (DOSs), which are shown in Fig. 2. First, we find in Fig. 2(a) that the A-site dependence of DOSs is very small, in particular near

 ©2018 American Physical Society

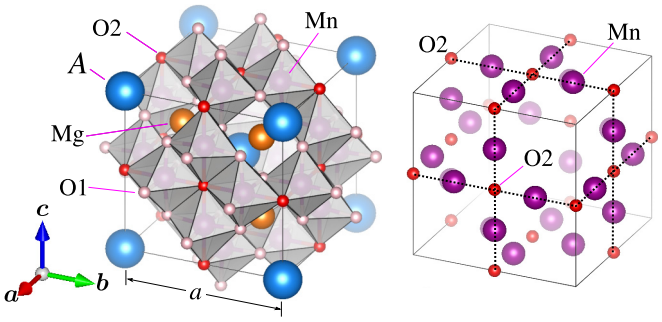

FIG. 1. Schematics of the crystal structure of $AMg_4Mn_6O_{15}$ (A = K,Rb,Cs). Atoms are distinguished by colors: A (blue), Mg (orange), Mn (purple), O1 (pink), and O2 (red). The 1D MnO chains are depicted in the right panel.

the Fermi level, which is consistent with experiment where no qualitative differences in their electronic properties have been observed among $AMg_4Mn_6O_{15}$ (A = K, Rb, and Cs) [16]. Hereafter, we will therefore discuss the electronic structure of $KMg_4Mn_6O_{15}$ only.

Next, we show the calculated partial DOSs for KMg_4-Mn_6O_{15} projected onto each ion in Fig. 2(b) where the spin polarization is allowed and $U = 0$ eV is assumed. We find that the $3d$ orbitals of Mn are fully spin polarized and form a half-metallic state where the majority-spin band crosses the Fermi level but the minority-spin band exhibits a large band gap. The calculated magnetic moment of $21\mu_B$ per primitive unit cell is consistent with experiment [16]. The opposite spin polarization of $2p$ orbitals of an O ion common in the negative charge-transfer-gap situation [4,23,24] does not occur in the present case.

Then, in Fig. 2(c), we show the calculated majority-spin partial DOSs projected onto each $3d$ orbital of a Mn ion at $U = 0$ eV. We find that the partial DOSs coming from the t_{2g} orbitals are well localized around -2 eV, whereas those from the e_g orbitals, the $d_{3z^2-r^2}$ orbital in particular, are rather extended between -1.5 and 1.5 eV. This dualistic nature, i.e., the presence of both localized and itinerant electrons in the same system, suggests that the ferromagnetism of this system may be caused by the double-exchange mechanism [10–13] just as in CrO_2 [24,25] and $K_2Cr_8O_{16}$ [4,5]. The same situation also occurs at $U = 4$ eV [see Fig. 2(d)]. We also note that the partial DOS curve of the Mn $3d_{3z^2-r^2}$ orbital exhibits the shape

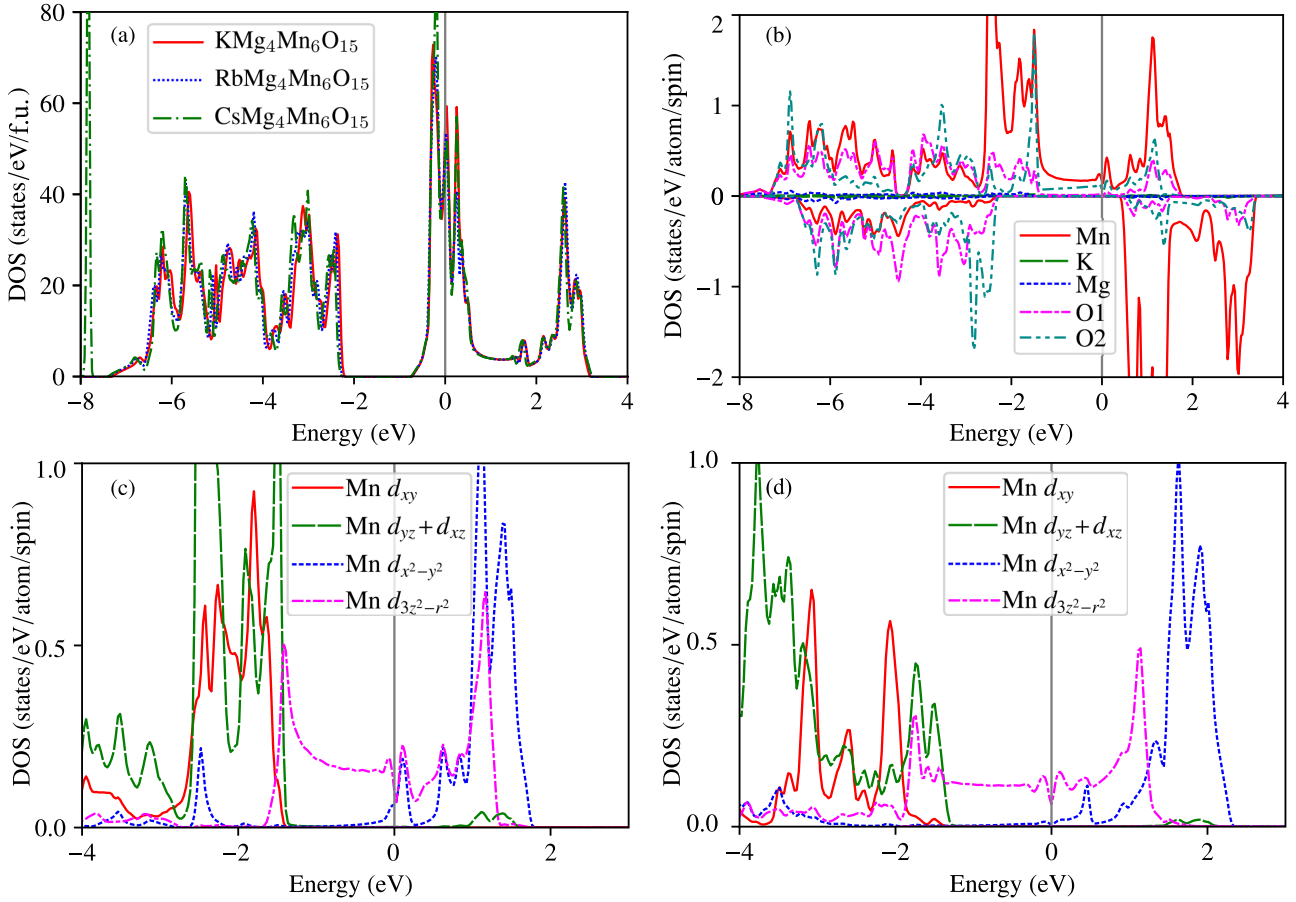

FIG. 2. Calculated total DOS and partial DOSs. (a) A-site dependence of DOS [per formula unit (f.u.)] for the hypothetical paramagnetic $AMg_4Mn_6O_{15}$ (A = K,Rb,Cs) at $U = 0$ eV. A sharp peak at -7.8 eV in A = Cs comes from the $5p$ orbital of a Cs ion. (b) Partial DOS projected onto each ion in ferromagnetic $KMg_4Mn_6O_{15}$ at $U = 0$ eV where the majority-spin (minority-spin) DOS is illustrated in the upper (lower) panel. A half-metallic situation is clearly seen. (c) Majority-spin partial DOS projected onto each $3d$ orbital of Mn in ferromagnetic $KMg_4Mn_6O_{15}$ at $U = 0$ eV. (d) The same as in (c) but at $U = 4$ eV. The vertical line in each panel represents the Fermi level.

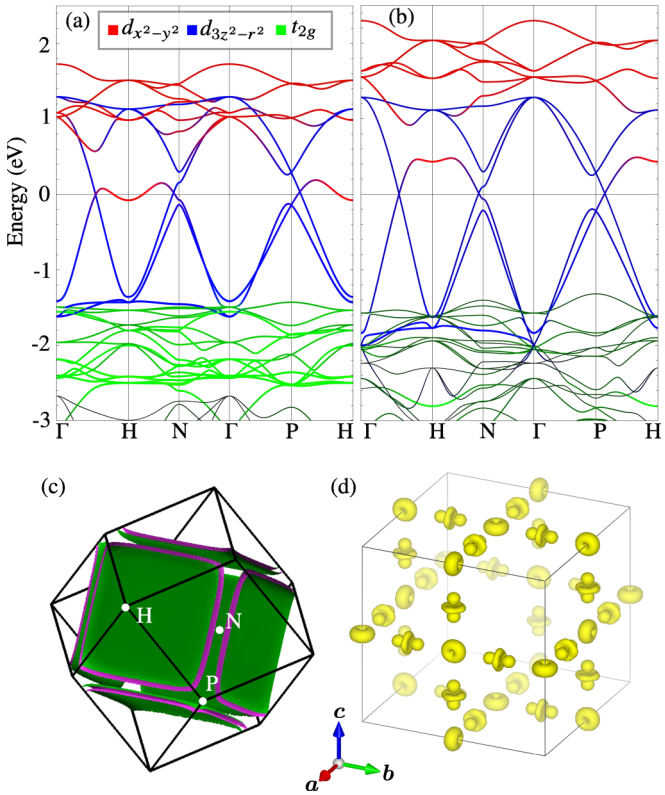

FIG. 3. Calculated majority-spin band dispersions for the ferromagnetic phase of $KMg_4Mn_6O_{15}$ at (a) $U = 0$ eV and (b) $U = 4$ eV where the red, blue, and green curves represent the weight of the $d_{x^2-y^2}$, $d_{3z^2-r^2}$, and t_{2g} contributions, respectively. The horizontal lines in each panel indicates the Fermi level. (c) Calculated Fermi surfaces for the ferromagnetic phase of $KMg_4Mn_6O_{15}$ at $U = 4$ eV. The constant energy surfaces of 25 meV below the Fermi level are illustrated so that the two sheets are slightly separated. (d) Calculated charge-density distribution in the energy window of ± 0.1 eV around the Fermi level. $U = 4$ eV is assumed.

of the DOS typical of the 1D tight-binding band, suggesting that the chain structure of Mn ions is formed in this system. We will discuss this aspect further below.

The calculated majority-spin band dispersions of $KMg_4Mn_6O_{15}$ are shown in Figs. 3(a) and 3(b) at $U = 0$ and $U = 4$ eV, respectively, where 6 red, 6 blue, and 18 green curves representing the $d_{x^2-y^2}$, $d_{3z^2-r^2}$, and t_{2g} contributions, respectively, are illustrated. We find that at $U = 0$ eV there is an electron pocket of the band coming predominantly from the $d_{x^2-y^2}$ orbital at the H point of the Brillouin zone. This band shifts upward with increasing U so that the electron pocket at the H point disappears at $U = 4$ eV. The bands forming the Fermi surfaces are thus predominantly from the $d_{3z^2-y^2}$ orbital.

Note that the two bands cross each other at the Fermi level, giving rise to the "surface-node" Fermi surfaces, which are three pairs of the parallel flat plates, as shown in Fig. 3(c). The flat plates are made of two sheets with the "nesting vector" $\boldsymbol{Q} = 0$, which indicates that when the unit cell contains more than two ions the Peierls instability causing the dimerization of ions may occur, keeping the unit cell unchanged. A good nesting feature of the nesting vectors $\boldsymbol{Q} \simeq (2\pi/a,0,0)$, $(0,2\pi/a,0)$, and $(0,0,2\pi/a)$ is also noted, indicating that the Peierls instability may also occur, which doubles the size of the unit cell of the system, i.e., from the body-centered-cubic structure to the simple-cubic structure (see below).

To envisage the electronic state of the system in real space, we calculate the density distribution of electrons ± 0.1 eV around the Fermi level. The result is shown in Fig. 3(d) where we clearly find that the $3d_{3z^2-r^2}$ orbitals of Mn and one of the three $2p$ orbitals ($2p_z$) of O2 form the 1D chain structure along the c direction of the cubic lattice. Similarly, we find the chain structures formed by the $3d_{3x^2-r^2}$ orbital of Mn and the $2p_x$ orbital of O2 along the a direction and by the $3d_{3y^2-r^2}$ orbital of Mn and the $2p_y$ orbital of O2 along the b direction of the cubic lattice. Note that the contributions from the O1 ions to the states near the Fermi level are very small.

Now, let us describe the low-energy electronic structure of this system by the tight-binding approximation where the atomic orbitals form the 1D chains as shown in Fig. 4(a). The unit cell contains the six $3d$ orbitals ($d_{3z^2-r^2}$ and its equivalents) of Mn and six $2p$ orbitals (p_z and its equivalents). The Hamiltonian for the majority-spin bands reads

$$\mathcal{H} = \varepsilon_d \sum_{i\mu} d^\dagger_{i\mu} d_{i\mu} + \varepsilon_p \sum_{i\mu} p^\dagger_{i\mu} p_{i\mu} + \mathcal{H}_{dp} + \mathcal{H}_{dd},$$

$$\mathcal{H}_{dp} = \sum_{\langle i\mu, j\nu\rangle} t^{pd}_{i\mu,j\nu} (d^\dagger_{i\mu} p_{j\nu} + \text{H.c.}),$$

$$\mathcal{H}_{dd} = \sum_{\langle i\mu, j\nu\rangle} t^{dd}_{i\mu,j\nu} (d^\dagger_{i\mu} d_{j\nu} + \text{H.c.}),$$

where $d^\dagger_{i\mu}$ creates an electron on the orbital μ at Mn site i and $p^\dagger_{j\nu}$ creates an electron on the orbital ν at O site j. $\langle i\mu, j\nu\rangle$ denotes the nearest-neighbor pair of orbital μ at site i and orbital ν at site j. ε_d and ε_p are the on-site energies of Mn $3d$ and O $2p$ orbitals, respectively, and t^{pd} and t^{dd} are the hopping integrals between the neighboring $2p$ and $3d$ orbitals and between the neighboring $3d$ orbitals, respectively. $\mathcal{H}_{dp}$ forms the 1D chains in the system, and $\mathcal{H}_{dd}$ introduces the coupling between the chains giving rise to the 3D ferromagnetism. We calculate the maximally localized Wannier orbitals using the method of Refs. [26,27], which provides a good fitting of the band dispersions in a wide energy range with a large number of the tight-binding parameters. However, we instead assume the values of $\varepsilon_p = -4.5$, $\varepsilon_d = -2.5$, and $|t^{pd}| = 2.2$ in units of eV and $t^{dd}/|t^{pd}| = -0.1$ for simplicity, which give accurate band dispersions at least near the Fermi level.

The tight-binding bands thus obtained are shown in Fig. 4(b) where the results for three cases are plotted: (i) only t^{pd} is included, (ii) both t^{pd} and t^{dd} are included, and (iii) t^{pd}, t^{dd}, and lattice dimerizations (adding a ± 0.2-eV alternation to t^{pd}, denoted as $\mathcal{H}_\Delta$) are included. We find that the inclusion of only the t^{pd} terms can reproduce the essential features of the bands, such as the crossing of the two bands at the Fermi level. We also find that the addition of the t^{dd} terms can explain the shift of the $\boldsymbol{k}$ point (from P to H) at which the two bands cross as well as the lifting of the band degeneracy. A better agreement with the results of the DFT-based band-structure calculations in a wider energy range down to around -2 eV is obtained if we take into account the hopping integrals between Mn and O1 ions [see Fig. 2(b)].

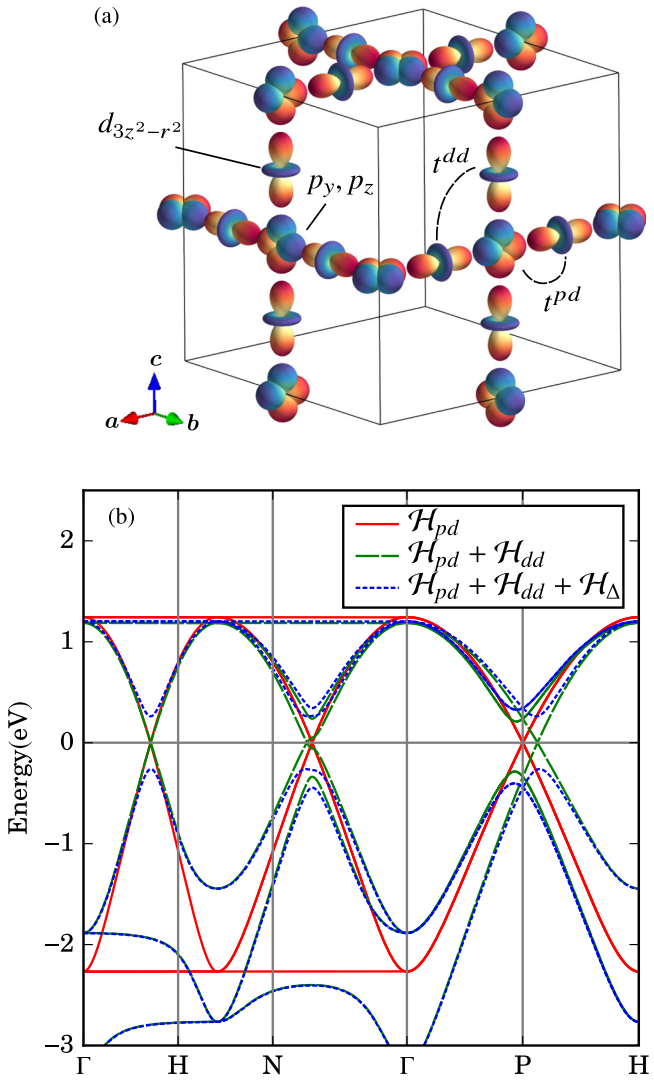

FIG. 4. (a) Schematic of the 1D chains of orbitals for $KMg_4Mn_6O_{15}$ where the orbitals $p_\alpha - d_{3\alpha^2-r^2} - p_\alpha - d_{3\alpha^2-r^2} - \cdots$ ($\alpha = x,y,z$) are illustrated. (b) Calculated majority-spin band dispersions of our tight-binding model where we assume only t^{pd} (red), both t^{pd} and t^{dd} (green), t^{pd}, t^{dd}, and lattice dimerizations with alternating ±0.2-eV modulations to t^{pd} (blue). Six $d_{3\alpha^2-r^2}$ bands, some of which are degenerate, are drawn in each case. For the lattice dimerization, we assume the pattern illustrated in Fig. 5(a).

Then, we find that the inclusion of the lattice dimerization actually leads to the opening of the band gap in the entire Brillouin zone, making the system insulating [see Fig. 4(b)]. There are a variety of spatial patterns of the lattice dimerization (or relative phase of the Peierls distortions), but the pattern is unique if we assume that the primitive unit cell does not change of which the pattern is illustrated in Fig. 5(a). If the primitive unit cell is extended (e.g., from the body-centered-cubic to the simple-cubic lattices), we may have different patterns of which an example is illustrated in Fig. 5(b). We performed the DFT-based band-structure calculations and checked that the band gap actually opens for the former pattern but the gap does not open for the latter of which the results are found to be consistent with our tight-binding model calculations. We also performed the structural optimization calculations based

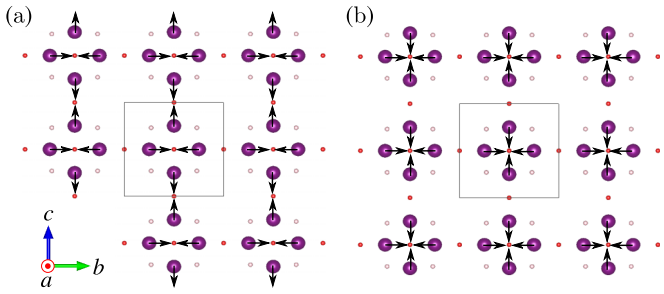

FIG. 5. Schematics of the lattice distortions (a) keeping the body-centered-cubic symmetry [space-group $Im\bar{3}$ (No. 204)] and (b) keeping only the simple-cubic symmetry [space-group $Pm\bar{3}m$ (No. 221)]. The [100] plane of the crystal, on which Mn ions are located, is illustrated. The arrows indicate the shifts of Mn ions along the 1D chain directions on the [100] plane.

on DFT where we assume the space-group $Im\bar{3}$ (No. 204) keeping the body-centered-cubic structure. We thus obtained the structural distortion as shown in Fig. 5(a) and confirmed the opening of the band gap. We hope that further experimental studies will be performed in the future to confirm the existence of the lattice distortion and to clarify what pattern is actually realized in the present materials.

Finally, let us discuss the finite-temperature behavior of $KMg_4Mn_6O_{15}$ in comparison with that of $K_2Cr_8O_{16}$. In the ground state, both materials are ferromagnetic insulators where the double-exchange mechanism leads to ferromagnetism and the Peierls mechanism leads to the band-gap formation. We should however point out that, above the transition temperature of the ferromagnetic insulator state, $K_2Cr_8O_{16}$ is a ferromagnetic metal, whereas $KMg_4Mn_6O_{15}$ is a paramagnetic insulator. The former situation is natural because we have a metallic band structure with the Peierls instability. However, the latter situation may also be possible if we consider the following: The uniform magnetic susceptibility of $KMg_4Mn_6O_{15}$ obeys the Curie-Weiss law [16], indicating that the local magnetic moment persists even at high temperatures [28–30]. In other words, the ferromagnetic spin correlation extends to a spatially wide region even in the paramagnetic state at $T > T_c$ so that the fully spin-polarized electronic state remains locally and hence the Peierls mechanism of the lattice dimerization works there. In fact, a slow ferromagnetic spin fluctuation above T_c has recently been observed by a muon spin rotation experiment [31]. The spin-fluctuation theory in the double-exchange ferromagnetism at finite temperatures should be developed in the future to quantify this argument.

Summarizing, we have used the DFT-based electronic structure calculations to study the electronic state of recently discovered mixed-valent manganese oxides $AMg_4Mn_6O_{15}$ (A = K,Rb,Cs), which are fully spin-polarized ferromagnetic insulators with a cubic structure at the lowest temperatures. We have shown that the system may be described as a 3D arrangement of the 1D chains of a $2p$ orbital of O and a $3d$ orbital of Mn running along the three axes of the cubic lattice. We have argued that in the ground state the chains are fully spin polarized due to the double-exchange mechanism and are distorted by the Peierls mechanism to make the system insulating. We have thus predicted the presence of the lattice

dimerization in the wide temperature range and the possible occurrence of the Peierls metal-insulator transition at a much higher temperature for which further experimental studies are desirable.

We thank T. Konishi, H. Okabe, T. Toriyama, and T. Yamauchi for useful discussions. This Rapid Communication was supported, in part, by a Grant-in-Aid for Scientific Research (Grant No. 17K05530) from JSPS of Japan.

[1] D. I. Khomskii, *Transition Metal Compounds* (Cambridge University Press, Cambridge, UK, 2014).
[2] D. I. Khomskii and G. A. Sawatzky, Solid State Commun. **102**, 87 (1997).
[3] K. Hasegawa, M. Isobe, T. Yamauchi, H. Ueda, J. I. Yamaura, H. Gotou, T. Yagi, H. Sato, and Y. Ueda, Phys. Rev. Lett. **103**, 146403 (2009).
[4] M. Sakamaki, T. Konishi, and Y. Ohta, Phys. Rev. B **80**, 024416 (2009); **82**, 099903(E) (2010).
[5] T. Toriyama, A. Nakao, Y. Yamaki, H. Nakao, Y. Murakami, K. Hasegawa, M. Isobe, Y. Ueda, A. V. Ushakov, D. I. Khomskii, S. V. Streltsov, T. Konishi, and Y. Ohta, Phys. Rev. Lett. **107**, 266402 (2011).
[6] A. Nakao, Y. Yamaki, H. Nakao, Y. Murakami, K. Hasegawa, M. Isobe, and Y. Ueda, J. Phys. Soc. Jpn. **81**, 054710 (2012).
[7] J. Sugiyama, H. Nozaki, M. Månsson, K. Prša, D. Andreica, A. Amato, M. Isobe, and Y. Ueda, Phys. Rev. B **85**, 214407 (2012).
[8] H. Takeda, Y. Shimizu, M. Itoh, M. Isobe, and Y. Ueda, Phys. Rev. B **88**, 165107 (2013).
[9] T. Yamauchi, K. Hasegawa, H. Ueda, M. Isobe, and Y. Ueda, Phys. Rev. B **92**, 165115 (2015).
[10] C. Zener, Phys. Rev. **81**, 440 (1951); **82**, 403 (1951).
[11] P. W. Anderson and H. Hasegawa, Phys. Rev. **100**, 675 (1955).
[12] P.-G. de Gennes, Phys. Rev. **118**, 141 (1960).
[13] P. Fazekas, *Lecture Notes on Electron Correlation and Magnetism* (World Scientific, Singapore, 1999).
[14] S. Nishimoto and Y. Ohta, Phys. Rev. Lett. **109**, 076401 (2012).
[15] S. V. Streltsov and D. I. Khomskii, Phys.-Usp. **187**, 1205 (2017); **60**, 1121 (2017).
[16] Y. Tanaka and H. Sato, J. Solid State Chem. **248**, 150 (2017).
[17] P. Blaha, K. Schwarz, G. K. H. Madsen, D. Kvasnicka, and J. Luitz, WIEN2K, *An Augmented Plane Wave Plus Local Orbitals Program for Calculating Crystal Properties* (Technische Universität Wien, Austria, 2001).
[18] J. P. Perdew, K. Burke, and M. Ernzerhof, Phys. Rev. Lett. **77**, 3865 (1996).
[19] V. I. Anisimov, I. V. Solovyev, M. A. Korotin, M. T. Czyżyk, and G. A. Sawatzky, Phys. Rev. B **48**, 16929 (1993).
[20] A. I. Liechtenstein, V. I. Anisimov, and J. Zaanen, Phys. Rev. B **52**, 5467(R) (1995).
[21] K. Momma and F. Izumi, J. Appl. Crystallogr. **44**, 1272 (2011).
[22] A. Kokalj, Comput. Mater. Sci. **28**, 155 (2003); http://www.xcrysden.org.
[23] D. I. Khomskii, Lithuanian, J. Phys. **37**, 65 (1997); arXiv:cond-mat/0101164.
[24] M. A. Korotin, V. I. Anisimov, D. I. Khomskii, and G. A. Sawatzky, Phys. Rev. Lett. **80**, 4305 (1998).
[25] H. Takeda, Y. Shimizu, Y. Kobayashi, M. Itoh, T. Jin-no, M. Isobe, Y. Ueda, S. Yoshida, Y. Muraoka, and T. Yokoya, Phys. Rev. B **93**, 235129 (2016).
[26] A. A. Mostofi, J. R. Yates, Y.-S. Lee, I. Souza, D. Vanderbilt, and N. Marzari, Comput. Phys. Commun. **178**, 685 (2008).
[27] J. Kuneš, R. Arita, P. Wissgott, A. Toschi, H. Ikeda, and K. Held, Comput. Phys. Commun. **181**, 1888 (2010).
[28] T. Moriya, *Spin Fluctuations in Itinerant Electron Magnetism*, (Springer-Verlag, Berlin, 1985).
[29] Y. Takahashi, J. Phys. Soc. Jpn. **55**, 3553 (1986).
[30] Y. Takahashi, *Spin Fluctuation Theory of Itinerant Electron Magnetism* (Springer-Verlag, Berlin, 2013).
[31] H. Okabe, M. Hiraishi, S. Takeshita, A. Koda, K. M. Kojima, R. Kadono, Y. Tanaka, and H. Sato (unpublished).